This is the Pre-Published Version.
R. Wadhwani, D. Sutherland, K. Moinuddin, X. Huang (2023) *Numerical simulation of two parallel merging wildfires*, **International Journal of Wildland Fire**. https://doi.org/10.1071/WF23071

Numerical simulation of two parallel merging wildfires

Rahul Wadhwani, Duncan Sutherland, Khalid Moinuddin[c], Xinyan Huang[a,*]

[a] *Research Centre for Fire Safety Engineering, Department of Building Environment and Energy Engineering, The Hong Kong Polytechnic University, Hong Kong*

[b] *School of Science, University of New South Wales, Canberra, Australia*

[c] *Institute of Sustainable Industries and Liveable Cities, Victoria University, Melbourne, Australia*

*Corresponding to xy.huang@polyu.edu.hk

Abstract:

Background: Wildfire often shows complex dynamic behaviour due to the inherent nature of ambient conditions, vegetation, and ignition patterns. Merging fire is one such dynamic behaviour that plays a critical role in the safety of structures and firefighters.

Aim & Method: The present study is a numerical validation of a physics-based CFD wildfire model concerning merging fires to develop better insight and understanding of the interaction of parallel merging firelines.

Conclusions: The validated model shows a relative error of 5-35% in estimating the rate of fire spread compared with the experimental observation in most of the cases. A physical interpretation is developed on how parallel fire behaves and interacts with the ambient conditions, providing complementary information to the experimental study.

Implications: The validated numerical model serves as a base case for further study in developing a better correlation for the rate of fire spread between parallel firelines with different ambient conditions, especially at the field scale.

Keywords: *parallel firelines; merging fire interaction; CFD simulations; wildfire spread; fire model validation; fire dynamics simulator (FDS); rate of fire spread; field scale*

Introduction

Wildfires are one of the major culprits in the devastation of the ecosystem, loss of vegetative coverage and biodiversity, and increment of greenhouse gas emission. The infamous 2019-20 Australian black summer wildfire season (Li *et al.* 2021) and the 2021 Siberian wildfires (Tomshin and Solovyev 2022) burned approximately 340,000 and 200,000 km^2 area, respectively. The Australian black summer season resulted in 34 direct fatalities, 445 fatalities attributed to smoke, and killed an estimated 3 billion vertebrate animals. An increasing number of dry days and severe drought exposure

due to climate change worsen the situation, promoting extreme fire behaviours (Parente *et al.* 2018; Halofsky *et al.* 2020). The dynamics controlling extreme wildfire behaviour are complex and still not completely understood (Sharples *et al.* 2011; Werth *et al.* 2011).

A key characteristic associated with this behaviour in many fuel types is dense spotting in which firebrands can transport from a few meters to kilometres downwind of the main firefront (Finney and McAllister 2011; Cruz *et al.* 2015; Manzello *et al.* 2020; Wadhwani *et al.* 2022). The presence of new fire spots (e.g., ignited by these firebrands) can cause an escalation in the overall rate of fire spread (ROS) and can cross natural or artificial firebreaks. This poses a serious risk to emergency personnel and the community involved. Coalescing of these spot fires could lead to more severe behaviour such as eruptive fire, firestorms, fire whirls, excessive firebrand activities, etc., which gives a multifold increase in the ROS (Werth *et al.* 2011; Sharples *et al.* 2016; Parente *et al.* 2018; Tedim *et al.* 2018).

In a regular fire in the absence of wind, buoyancy-driven air entrainment occurs symmetrically from all directions, which makes the fire plume upright. However, when multiple fires burn or the fire fronts are close enough to interact (as shown in Fig. 1), the plume-induced airflow is contested among the fire spots and firelines, and air entrainment is restricted. As a result, there is a pressure drop along the line connecting the fire plumes, making the fires tilt towards each other. This phenomenon is called merging fires. When there is a driving wind the situation is more complicated, however, the interaction of the buoyant plumes can still result in a pyrogenic wind between the two fire lines which serves to entrain fresh air from outside the fire which results in the fire lines being pushed together. Merging fires can be classified into three categories: coalescing, junction and parallel fires based on the approach of fireline contours, as shown in Fig. 1. Convergence of multiple independent fire spots is called coalescing while the convergence of two fire fronts at some oblique angle is called junction fire and at zero degrees angle is called parallel fire. While the geometry of the particular fire merger complicates the dynamics, the overall principle of plume interaction leading to a pyrogenic wind that draws the fire lines together remains.

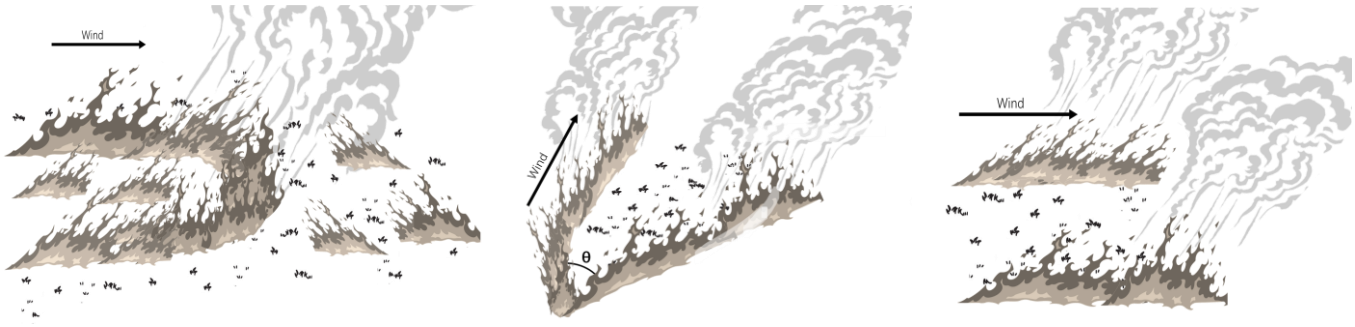

(a) Coalescing fires (b) V-shaped junction fires (c) Parallel fires

Fig.1: Cartoons of different categories of merging fires: (a) coalescing, (b) V-shaped junction, where θ is the angle between two firelines, and (c) parallel fires. Here the grey regions represent flaming regions, the white regions with blades of grass (black) represents unburnt areas.

The merging fires have been studied by various researchers in the past couple of decades. Liu *et al.* (2021) have reviewed many such studies and discussed the mechanism of fire behaviour in merging fires. In its early years, the focus was on operational purposes especially the utilisation of parallel fire for back-burning operation tactics to contain the fire spread. It was observed that interaction between the two (forward and backwards) fires occurs only at short distances (Sullivan *et al.* 2019). Morvan *et al.* (2011) carried out a numerical simulation study to understand the aforementioned behaviour between two parallel fire fronts on a flat grassland fuel bed, and a wind direction perpendicular to the firelines. They also observed a similar behaviour of interaction as observed in back-burning operations.

Other researchers mainly studied the V-shape fire experimentally and numerically as it is frequently observed in a wildfire (Viegas *et al.* 2012; Viegas *et al.* 2013; Thomas *et al.* 2017; Sullivan *et al.* 2019; Hassan *et al.* 2023). However, understanding the behaviour controlling the interacting parallel fire propagating in the presence of wind is limited. There is ample evidence of such interaction between parallel fire fronts. Some prominent examples are the 1980 Chachukew fire (De Groot and Alexander 1986), Canada, the 1987 Heathcote fire, Australia (Billing 1987), the 2002 Hayman fire, USA (Graham 2003), the 2003 Canberra fire, Australia (Blanchi and Leonard 2005), the 2016 Fort McMurray fire (Ronchi *et al.* 2017), and the 2017 Quiaios wildfire, Portugal (San-Miguel-Ayanz *et al.* 2020; Ribeiro *et al.* 2022).

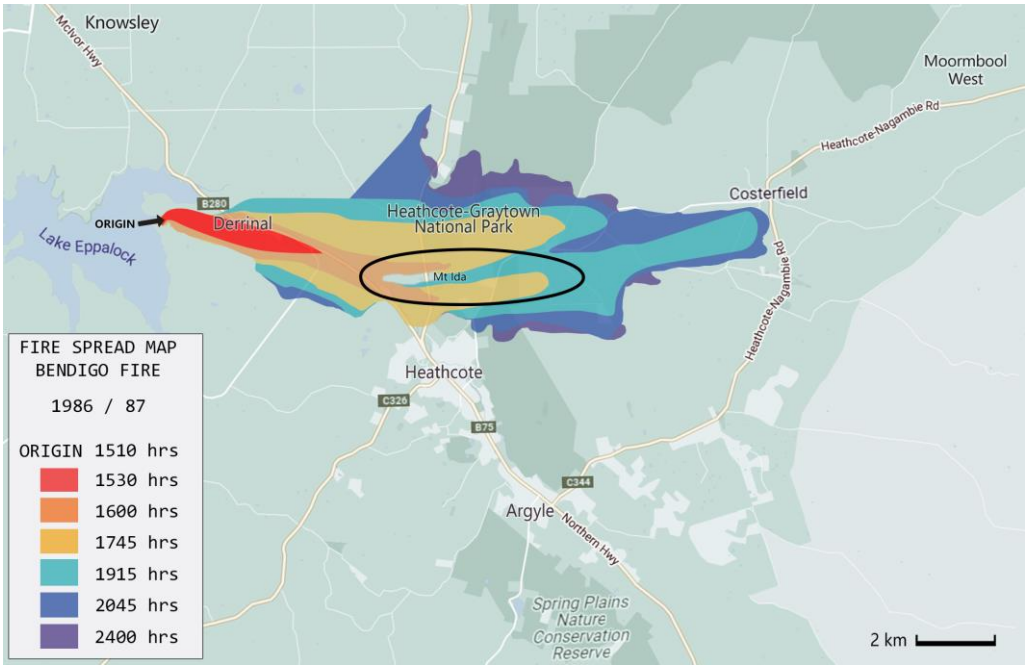

Fig. 2: Evolution of fire perimeter of Heathcote fire, Australia observed on 16th January 1987. Black highlighted area shows parallel fire behaviour. Fire spread map adapted from Biling (1987).

The Heathcote fire, Australia is one of the detailed incidents available in the public domain which highlighted an interacting run of two parallel grassfires for approximately 4.5 hours and is shown in Fig. 2 (highlighted in black) (Billing 1987). In the Heathcote fire, the fire ignited in grassland at 1510

hrs on 16th January 1987 probably due to faulty motorcycle exhaust. The extreme ambient conditions fanned the fire in grassland approximately at 11km/hr ROS towards the populated area of Heathcote. Around 1545 hrs, 2 km away from the suburb a change in the wind direction caused fragmentation of the head fire front near Mount Ida. The fragmented front continued to burn until 2000 hrs and was approximately 1 km apart before merging. Despite the slowed ROS due to high fuel moisture, lower vegetation distribution and milder wind conditions, it was a challenge to control the fire propagation.

Thus, developing a better understanding of the dynamics of parallel behaviour and the impact of ambient conditions on fire spread is crucial. Recently, two experimental studies (Filkov *et al.* 2020; Ribeiro *et al.* 2022) have been carried out to understand the dynamics behind the parallel fire on a limited set of ambient conditions. Experimental studies are expensive which requires measuring devices, equipment, manpower, fire safety protocols and can be carried out only on a limited set of ambient conditions with very limited control on those conditions. A numerical approach to understanding this phenomenon would be a cost and time-effective and better-controlled study which is the objective of the present work.

Simulation domain and boundary conditions

Ribeiro *et al.* (2022) carried out a set of experiments in a combustion tunnel to study the interaction between two parallel firelines with a working area of 8 × 6 m^2. The fuel bed composed of straw (*Avena sativa*) of height 0.07m was spread in an area of 5 × 4 m^2 (as shown in Fig. 3). They conducted twelve experiments by varying uniform mean wind speed (U_0) of 0, 1, 2, 3, 4, 5 m/s and the varying spacing between the two firelines to values of 1 and 2 m. The length of fireline was constant at 2 m long. Properties of the fuel used in the present study are detailed in Table 1 while other properties and experimental protocol including the experimental measurement techniques can be found in Ribeiro *et al.* (2022). A diagram of the simulation setup is shown in Fig. 3.

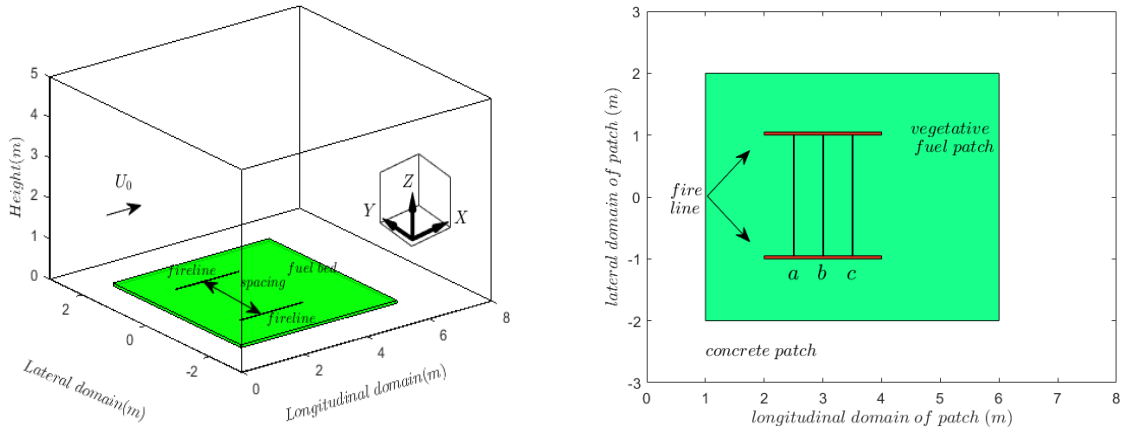

(a) Simulation setup (b) Measuring sites for ROS

Fig. 3: Simulation setup and measuring sites of ROS for Ribeiro *et al.*'s experiment where U_0 represents the direction of the wind

Some fuel properties were assumed or taken from the literature in the present study due to a lack of data. Australian grassfire thermo-physical and chemical properties are used to represent straw fuel beds in the present study (McGrattan *et al.* 2022a). Soot yield and emissivity data for the present study are assumed to be similar to that of Australian Lucerne hay straw (Wadhwani 2019). The heat release rate per unit area (HRRPUA) of fireline is assumed to be 250 kW/m^2 based on the HRRPUA similar material (Hurley *et al.* 2015). Ribeiro *et al.* (2022) measured the rate of fire spread (ROS) between the two parallel firelines along the three lines marked as 'a', 'b', and 'c' (shown in Fig. 3(b)) at the longitudinal position of 2.5, 3, and 3.5 m respectively. The ROS (denoted as $R_a, R_b,$ and R_c) is measured along the line 'a', 'b', and 'c' by recording the successive movement of the fireline in 5-s interval. They assumed that the ROS from both fire fronts was symmetrical.

Table 1: Fuel properties used in the present study.

Fuel Parameter	**Values**	**Reference**
Vegetative fuel	Straw (*Avena sativa*)	(Ribeiro *et al.* 2022)
Fuel load	600 g/m^2	
Packing ratio	0.029	
Fuel height	0.07 m	
Surface area to volume ratio	4734 m^{-1}	
Moisture content	Supplementary document	
Heat of combustion	18,000 kJ/kg	
HRRPUA_fireline	250 kW/m^2	(Hurley *et al.* 2015)
thermal conductivity - straw	0.11 W/m.K	(Vanella *et al.* 2021; McGrattan *et al.* 2022a)
Heat capacity – straw	1.5 kJ/kg.K	
A_{py} (pyrolysis)	36,300 s^{-1}	
E_{py} (pyrolysis)	60,300 J/mol	
A_{dr} (drying)	600,000 K$^{0.5}$s^{-1}	
E_{dr} (drying)	48,200 J/mol	
A_{char}(Char oxidation)	430 m/s	
E_{char}(Char oxidation)	74,800 J/mol	
Emissivity	0.98	(Wadhwani 2019)
Soot yield	0.02 kg/kg	
Boundary and Mesh Conditions		
Simulation domain	x= 0-8 m, y= -3-3 m, and z= 0-5 m	(Ribeiro *et al.* 2022)
Vegetative fuel patch	x= 1-6 m, y= -2-2 m, and z= 0-0.07 m	
Fireline location	x=2-4 m, for 1 m spacing: y=±0.5 m; for 2 m spacing: y=±1 m	
Grid size	$\Delta x = \Delta y = \Delta z$ =0.025 m	(Perez-Ramirez *et al.* 2017)
Grid convergence test	Fine: $\Delta x = \Delta y = \Delta z$ =0.0125 m Coarse: $\Delta x = \Delta y = \Delta z$ =0.05 m	

The numerical simulation of the experimental setup was carried out with Fire Dynamics Simulator (FDS ver. 6.7.8) (McGrattan *et al.* 2022a). The boundary fuel model was used to represent the vegetative fuel bed in the present study and the governing equation are discussed in the subsequent section. The wind was defined at X=0 m with a mean uniform wind speed of 0-5 m/s, and to represent a realistic experimental scenario, turbulence is introduced at the wind inlet. A perturbation is introduced using the synthetic eddy method (described in detail by Jarrin (2008)) to represent turbulence at the entrance. The perturbation wind speed was assumed to be 10% of the mean wind speed to be commensurate with typical wind turbulence intensities (McGrattan *et al.* 2022a). The Z= 0 m was defined with a no-slip boundary while other boundaries were fixed as constant pressure open boundaries. The grid resolution was selected to ensure that the flow and radiation equations were adequately resolved; this was tested with a convergence study.

Governing Equations and Sub-models

FDS has broadly three model approaches to describe vegetative fuel: particle model, boundary fuel model, and level-set method model (details are available in (McGrattan *et al.* 2022a)). In the particle model, the vegetative fuel bed is defined as a collection set of Lagrangian particles, which requires sufficient grid resolution to resolve convective and radiative heat transfer for head fire propagation. The boundary fuel model represents fuel as a porous solid layer with a thickness equal to fuel height. The surface vegetation layer is too shallow to be resolved explicitly, as is done when using Lagrangian particle model to represent the vegetation.

The fire propagation is assumed to dominate mainly by radiation, and the height of vegetative fuel is also assumed to be unresolved on the grid. The level set method model is based on empirical fire models and the thermal degradation or combustion of fuel is not considered, unlike the other two models. Recently, Vanella *et al.* (2021) tested the efficacy of the above three models for Australian grassfire experiments C064 and F19 conducted by Cheney *et al.* (1993). They found that the particle and boundary fuel model gave close agreement with the field experimental data. The boundary fuel model is selected in this work to represent vegetative fuel as it is not significantly computationally expensive in representing vegetation. The model has been widely tested and validated in the past at various scales and sizes (Mell *et al.* 2007; Morvan *et al.* 2011; Mell *et al.* 2013; Perez-Ramirez *et al.* 2017; Khan *et al.* 2019; Moinuddin and Sutherland 2019; Wadhwani 2019).

The thermal degradation of vegetative fuel inside the boundary fuel model is described by following three equations.

1. Endothermic evaporation of moisture

$$\text{Wet fuel} \rightarrow \vartheta_{H_2O} \cdot H_2O + \left(1 - \vartheta_{H_2O}\right) \cdot \text{Dry fuel}, \ \vartheta_{H_2O} = \frac{M}{1+M}, \qquad \text{Eq. 1}$$

2. Endothermic pyrolysis of dry vegetation. It controls how much fuel gases are released from the fuel to the flame.

$$\text{Dry fuel} \rightarrow \vartheta_{char} \cdot Char + (1 - \vartheta_{char}) \cdot \text{ fuel gases}, \quad \text{Eq. 2}$$

3. Exothermic oxidation of char (or smouldering)

$$\text{Char} + \vartheta_{O_2,char} \cdot O_2 \rightarrow \left(1 + \vartheta_{O_2,char} - \vartheta_{ash}\right) \cdot CO_2 + \vartheta_{ash} \cdot \text{ Ash}, \quad \text{Eq. 3}$$

where, M is the moisture content determined based on the dry fuel mass basis. $\vartheta_{O_2,char}$ is the mass of oxygen required per unit mass of char consumed, ϑ_{char} is the mass fraction of dry vegetation that is converted to char during pyrolysis, and ϑ_{ash} is the mass fraction of char that is converted to ash during the char oxidation process. The reaction kinetics of the above set of reactions are given in Table 1.

The drag exerted by the porous surface vegetation is modelled using a drag term in the momentum equation, and convective heat transfer is modelled via a source term in the one-dimensional heat conduction equation that is solved through the layer of vegetation and solid ground. Thermal radiation penetrates the vegetation layer via a 1D radiative heat transport equation that is used for semi-transparent solids. The drag exerted on the wind flowing through the vegetation is imposed as a force term (f_b) in the gas phase grid cell adjacent to the boundary and is defined by Eq. 4.

$$f_b = \frac{\rho}{2} C_d C_s \beta \sigma' \frac{h_b}{\delta z} \boldsymbol{u}||\boldsymbol{u}||, \quad \text{Eq. 4}$$

where, ρ is the density of air, C_d is the drag coefficient, C_s is the shape factor (ratio of projected area to surface area), β is the packing ratio, σ' is the surface area to volume ratio, h_b is the depth of vegetation, δz is the height of the grid cell, and $\boldsymbol{u}$ is the air velocity in the first grid cell.

Thermal radiation is absorbed in depth according to a 1D radiative transport solver. The absorption coefficient (κ) is given by,

$$\kappa = C_s \sigma' \beta, \quad \text{Eq. 5}$$

Thermal convection is not imposed at the interface between the gas phase and the vegetation layer, but rather imposed via a source term in the 1D heat conduction solver:

$$\dot{q}'''_{c,b} = \dot{q}''_c \sigma' \beta, \quad \text{Eq. 6}$$

where, $\dot{q}''_c$ is the convective heat transfer to the surface, which is given by,

$$\dot{q}''_c = h(T_g - T_s), \quad \text{Eq. 7}$$

where, h is the heat transfer coefficient, T_g is the gas temperature taken from the first gas phase grid cell adjacent to the boundary, and T_s is extracted from the solution of the 1D heat conduction equation. For a more extensive discussion see McGrattan *et al.* (2022b).

Results and Discussion

The numerical set-up of Ribeiro *et al.*'s experiment is already presented in Fig. 3, and the fuel properties and boundary conditions are already discussed in previous sections. The simulation initially

ran for 30 s to establish a flow field in the entire simulated domain. This was to provide steady-state wind conditions before the ignition of two parallel firelines. The fireline was ignited with an HRRPUA of 250 kW/m^2 to represent the experimental ignition of the fuel bed.

When the ignition of the fuel bed occurs initially the firelines are straight lines but transform into a curve when they spread under the influence of horizontal force (along the X axis) of wind and vertical force (along the Z axis) of buoyancy. The fuel bed temperature was assumed to be a representative of a fire front which has been used in various previous studies using physics-based fire models (Linn *et al.* 2002; Mell *et al.* 2007; Sullivan 2009; Morvan *et al.* 2011; Mell *et al.* 2013; Perez-Ramirez *et al.* 2017; Moinuddin *et al.* 2018; Khan *et al.* 2019). Two types of fire fronts were assumed in the present study, a pyrolysis front where the temperature of the fuel bed is above 120 °C, and a burning fire front where the temperature of the fuel bed is above 400 °C (Mell *et al.* 2007; Morvan *et al.* 2011; Perez-Ramirez *et al.* 2017). The rate of fire spread (ROS) was quantified by measuring the successive movement of the location of fuel bed temperature peak in the burning fire front along measuring lines.

Fig. 4 shows the evolution of fire for a 2 m spaced parallel firelines at two wind speeds ($U_0 =$ 0 & 5 m/s) as they represent two extreme flow conditions of the present study. An interaction between the two parallel firelines was observed as the growth of fire was not symmetrical around the firelines even when wind speed was zero. The growth and merging of two firelines in $U_0 = 0$ m/s (Fig. 4(a)-(d)) situation was buoyancy driven. The flame of parallel firelines was upright at t= 39s (Fig. 4(a)) and starts to incline ~t= 45 s (Fig. 4(b)) which grows further as can be seen in Fig. 4(c) (~t= 54s).

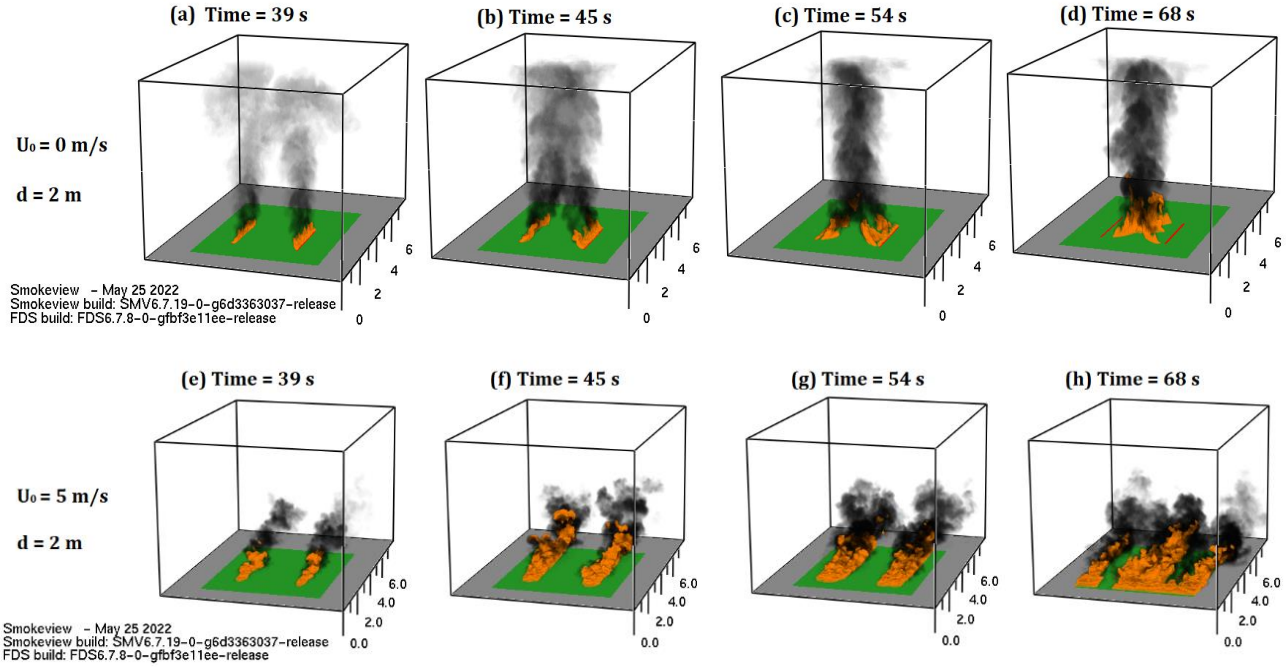

Fig. 4: Evolution of fire spread observed with the heat release rate per unit volume (more than 200 kW/m^3) for two wind conditions (a)-(d) for $U_0 = 0$ m/s and (e)-(h) for $U_0 = 5$ m/s using Smokeview.

The inward tilt of fires naturally enhances the radiant heat feedback because the view factor between the fire's increases. Thus, increasing the ROS. While the growth of fire in $U_0 = 5$ m/s (Fig. 4(e)-(h)) was a combined effort of the shear force of the wind by increasing convective and radiative heat transfer, increased burning of fuel bed due to more availability of oxygen, and the buoyancy force. The behaviour of fire was significantly turbulent due to strong wind speed when compared with zero wind speed scenarios. Due to higher fire intensity and significant contribution by radiant and convective heat transfer, the fire spreads all over the vegetative fuel.

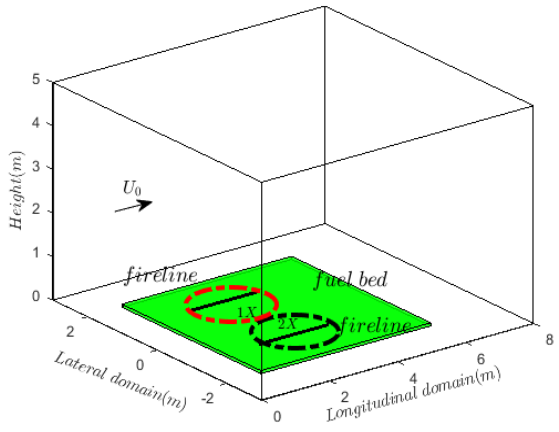

(a) Two nomenclature 1X and 2X used for measuring the ROS

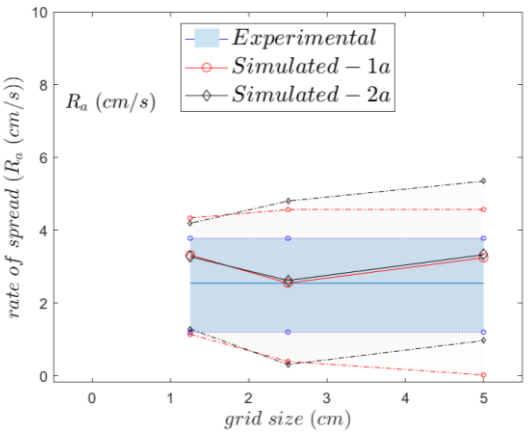

(b) R_a

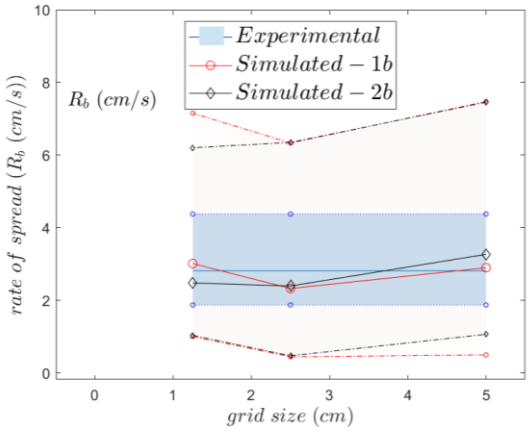

(c) R_b

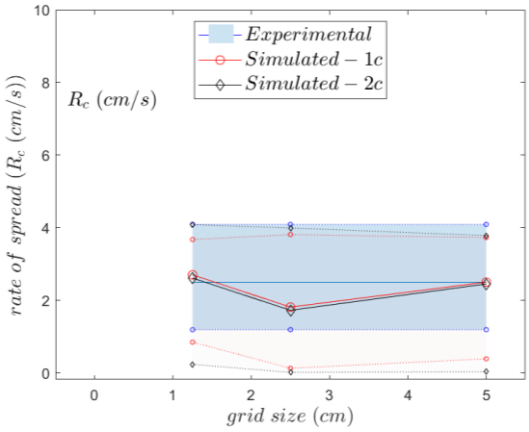

(d) R_c

Fig. 5: Grid convergence test for $U_0 = 0$ m/s by comparing the ROS measured along the three lines 'a', 'b', and 'c'. The mean ROS is presented by solid lines (the blue line without marker represents - experimental data, red and black with markers represent - simulated data for 1X, 2X, (X=a, b, and c)) and the dotted line represents the maxima/minima of ROS for each measurement.

The grid convergence results were carried at three grid sizes (discussed in Table 1) at two wind speed conditions i.e., $U_0 = 0$ & 5 m/s for the spacing between the two firelines of 2 m as it considers both scenarios of fire spread. In the present study, it was not assumed that fire spread was symmetrical

and was measured from both sides of parallel firelines. They were marked as 1X and 2X, where X=a, b, and c representing measurement along the lines 'a', 'b', and 'c', and is shown in Fig. 5(a) and Fig. 3(b). Fig. 5(b)-(d) and Fig. 6 show the variation of the ROS along three measuring lines with different grid sizes. The shaded region highlights the maximum and minimum ROS observed.

A very good agreement between the modelled and the experimental mean ROS along the measuring lines was observed for all three grid sizes for $U_0 = 0$ m/s in Fig. 5(b)-(d). Specifically, the relative error between the experimental and simulated mean ROS is less than 25%. A higher value of the maximum and minimum ROS (especially for (R_b)) was observed due to the temporal resolution of simulation data processed giving further insight into the merging behaviour of two parallel fire fronts. The simulated data was measured at every 0.1s and was averaged over 10 points to compute rate of spread while the experimental measurement is carried out at an interval of 5 s.

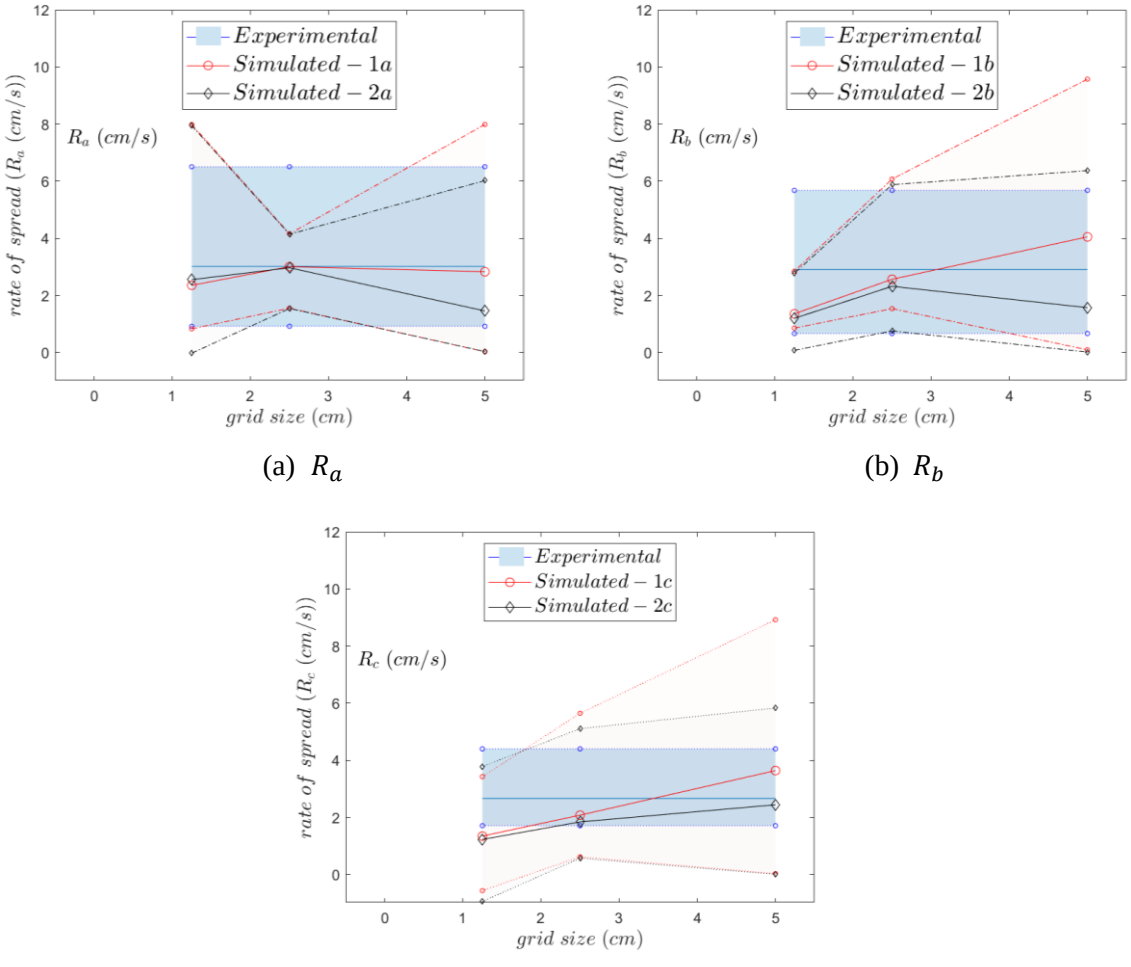

(a) R_a (b) R_b

(c) R_c

Fig. 6: Grid convergence test for $U_0 = 5$ m/s by comparing the ROS measured along the three lines 'a', 'b', and 'c'. The mean ROS is presented by solid lines (the blue line without marker represents - experimental data, red and black with markers represent - simulated data for 1X, 2X, (X=a, b, and c)) and the dotted line represents the maxima/minima of ROS for each measurement.

The modelling results observed by grid sizes of 0.025 and 0.05 m both were comparable to experimental observations. At grid resolution of 0.025 m comprising 15.36 million grid cells required 4 nodes of 16 GB each for ~96 hrs to simulate computational time of 2 mins. Similarly, in Fig. 6 for $U_0 = 5$ m/s, the results were close to experimental observation for grid sizes of 0.025 and 0.05 m, however, the results were found to be further away for R_b & R_c from the experimental observation due to inaccurate resolution of turbulence of near-surface wind speed which is highlighted in Fig. 7 (discussed more subsequently). This issue has a more profound impact when a fine grid scale (i.e., grid size = 0.0125 m) was considered. It can be concluded from both grid-convergence studies that grid size $\Delta x = \Delta y = \Delta z$ =0.025 m shows a good comparison with the experimental data and less maximum and minimum variation. The supplementary file provides comparative results with a grid size of 0.05 m.

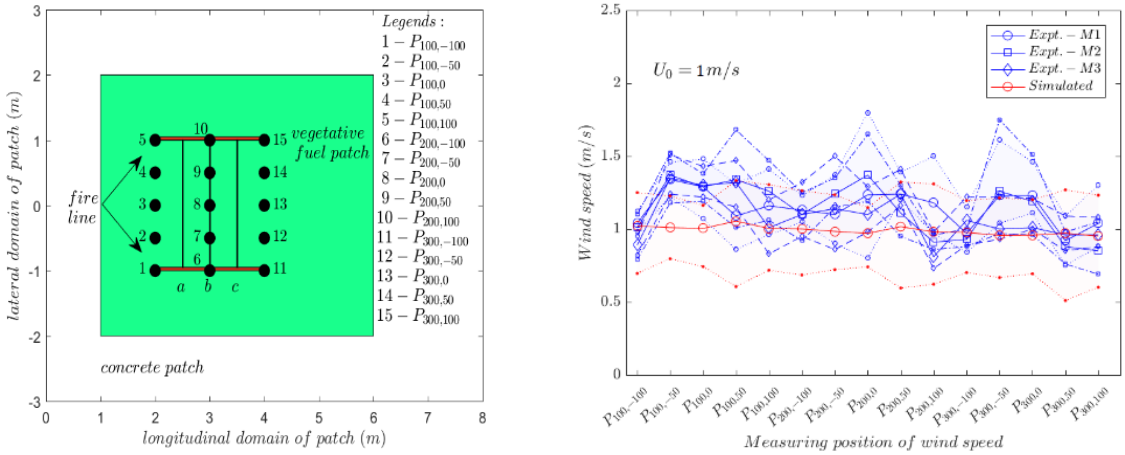

(a) Measuring site of near-surface wind measurement in the experiment

(b) Near-surface wind speed comparison at $U_0 = 1$ m/s

(c) Near-surface wind speed comparison at $U_0 = 3$ m/s

(d) Near-surface wind speed comparison at $U_0 = 5$ m/s

Fig. 7: Comparison of near-surface wind speed between three experimental runs (M1-M3) and simulation at various positions in between the firelines at three different wind speeds. The shaded area between dotted lines represents the maximum and minimum wind speeds.

Fig. 7 shows the comparison of near-surface wind speed across the domain, the location and legend for measuring location are presented in Fig. 7(a). Fifteen measuring sites are considered as shown in Fig. 7(a) and are labelled as $P_{m,n}$ where m is the location in the longitudinal direction and n is the location in the lateral direction. The near-surface wind measurement is carried out 22 cm above the fuel bed. The simulated near-surface wind speed is found to be close to the three experimental measurements (M1-M3) reported by Ribeiro *et al.* (2022). Fig. 7 shows that range of simulated wind speeds are within the range observed in the experimental study.

The turbulence in the wind speed measured during the experiment is found to be higher than simulation, reflected by the observed wind speed fluctuations being higher than the simulated wind speed fluctuations. The isotropic synthetic eddy method (Jarrin 2008) used in the present study is not sufficient enough to replicate experimental turbulence. The anisotropic synthetic eddy method (Jarrin 2008) could have been used to improve the accuracy, however, it requires a detailed experimental measurement of turbulence which was not available from the experiment.

The interaction between near-surface wind and fuel structure could also be the reason for the difference between experimental and simulated studies. The accurate measurement of near-surface wind has a significant impact on the estimation of the ROS which should be a consideration in future experiments. This inaccuracy of not accounting for turbulence becomes significantly profound when $U_0 = 5$ m/s case is considered, at fine grid size ($\Delta x = \Delta y = \Delta z$ =0.0125 m) a negative value for the minimum rate of spread was observed when two firelines approached (negative value of the ROS indicates the opposite direction in which the peak instantly progressed).

Fig. 8 and Fig. 9 show the ROS estimated by simulation and its comparison with the corresponding ROS measured during the experiments when the spacing between two firelines was 1 m and 2 m respectively (the supplementary file provides results observed with coarse grid size). The measurement was carried out along three measuring lines (Refer Fig. 7(a)) along both lateral directions (Refer Fig. 5(a)). The mean ROS was found to be closer to the experimental mean ROS along three measuring lines. Ribeiro *et al.* (2022) provided the result in the non-dimensional form of ROS which is the ratio of ROS observed in merging fire to the ROS observed in a single line fire. Unfortunately, the detail provided was not sufficient enough to reproduce such value numerically. Thus, we have compared with their experiments.

The relative percentage error (ε_{R_i}) (Eq. 8) found for the mean ROS along three measuring lines for two spacing distances between the firelines are given in Table 2.

$$\varepsilon_{R_i} = \frac{|\bar{R}_{i,sim} - \bar{R}_{i,expt}|}{\bar{R}_{i,expt}} \times 100, \qquad \text{Eq. 8}$$

where, i is a suffix suited to represent measurement along the measuring lines ‘a’, ‘b’, and ‘c’, $\bar{R}_{i,expt}$ and $\bar{R}_{i,sim}$ are the mean ROS measured along the measuring lines.

From Table 2, it can be seen most of the relative percentage errors were found to be in the range of 5-35% with some cases exhibiting a very good fit with the experimental measurements. A few cases showed exceptionally high values of error (70-94%) which was mainly due to a significantly small experimental ROS. It was also observed that the behaviour of approaching fire fronts was non-monotonic i.e. one fire line will tend to accelerate or decelerate as it approaches the other fire line (Viegas *et al.* 2021). It can be observed that the simulated ROS was not perfectly symmetric (i.e. 1X ≠ 2X) as assumed by Ribeiro *et al.* (2022) in their study. Though for most cases, 1X was approximately equal to 2X which can be seen in Fig. 8 and 9.

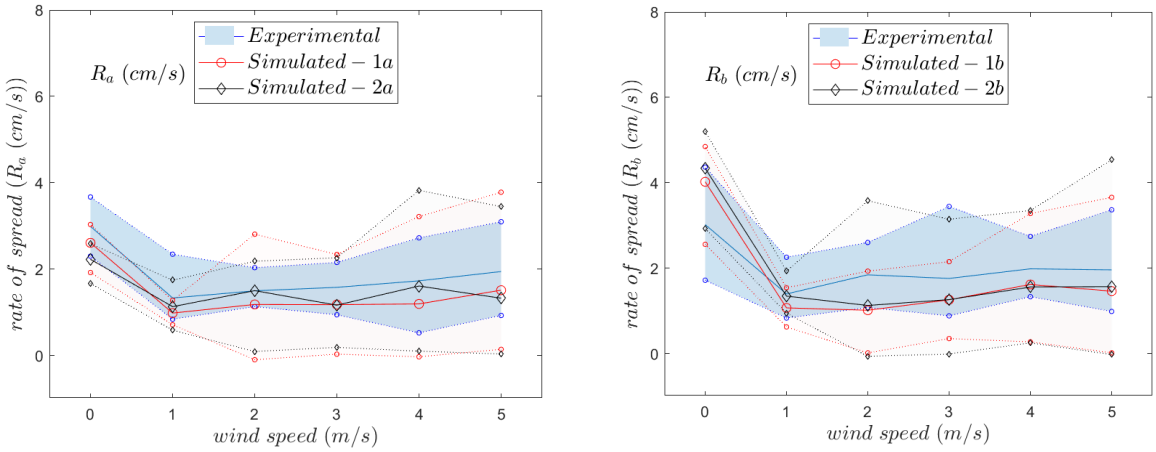

(a) R_a (b) R_b

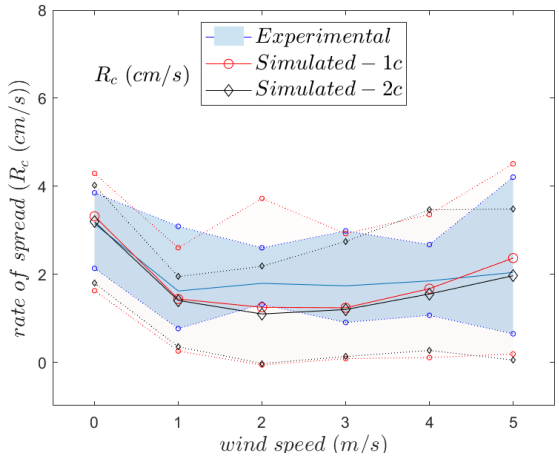

(c) R_c

Fig. 8: Comparison of ROS observed from simulation and experiment by measuring along 'a', 'b', and 'c' at different wind speeds for spacing between two parallel firelines of 1 m. The mean ROS is denoted by solid lines (blue without marker represents - experimental data, red and black with markers represent - simulated data for 1X, 2X, (X=a, b, and c)) and maximum/minimum ROS is represented by the shaded area between dotted lines.

For wind speed $U_0 = 0$ m/s case, the fire lines were mainly driven towards each other by buoyancy, in the absence of external wind shear stress along the X-axis. The limited availability of oxygen between the two firelines was responsible for driving fire lines towards each other. A tilt in

flame angle is observed which is shown in Fig. 4(b)-(c) (similarly in Fig. 10(b)-(c)) for 2 m spacing as fire entrained towards each other. Fig. 10 further highlights this aspect by visualising the streamlines along the measuring line 'b', i.e., $X = 3\ m$, and pressure variation shown in Fig. 4(a)-(d).

A higher value for the ROS was observed between the fire lines, in zero wind conditions, than compared to the situation where the horizontal wind is present such as $U_0 = 1$ & 2 m/s. When the two firelines start to burn, the flames lean towards each other increasing the radiative heat transfer in pre-heating the fuel bed and approaching faster toward each other in the initial phase. Later, the in-draft by the burnt area on the fireline slightly reduces the ROS before they merge and makes the flame angle vertical. Further, it was also observed that a higher value of the ROS was found at the lower spacing between the firelines. The spacing seems to play a vital role in affecting the ROS as the effect of radiant heat and tilted flame in preheating the fuel bed start at early as compared to a large spaced fireline.

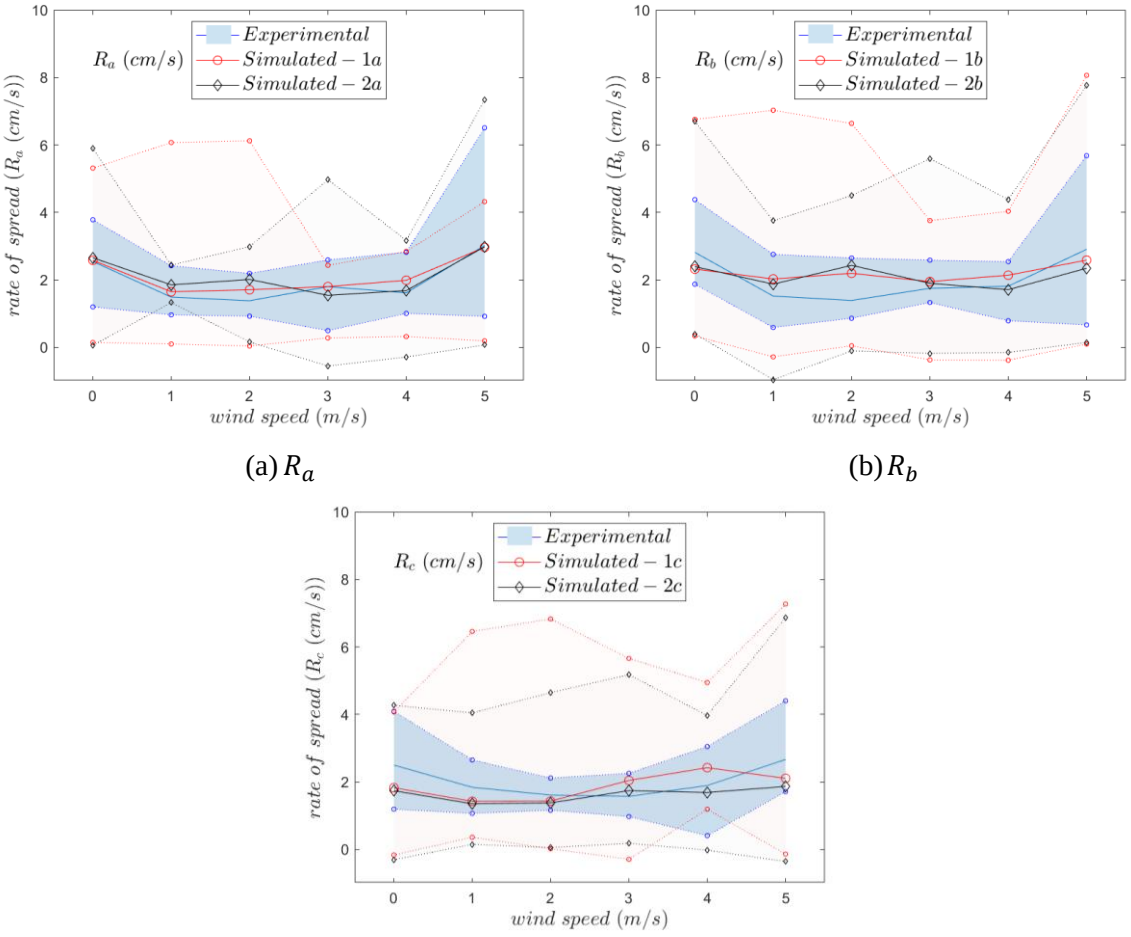

(a) R_a (b) R_b

(c) R_c

Fig. 9: Comparison of ROS observed from simulation and experiment by measuring along 'a', 'b', and 'c' at different wind speeds for spacing between two parallel firelines of 2 m. The mean ROS is denoted by solid lines (blue without marker represents - experimental data, red and black with markers represent - simulated data for 1X, 2X, (X=a, b, and c)) and maximum/minimum ROS is represented by the shaded area between dotted lines.

Table 2: Absolute relative percentage error in estimating the ROS along three measuring lines ‘a’, ‘b’, and ‘c’.

Wind speed (U_0) (m/s)	ε_{R_a} (%) 1a[2a]		ε_{R_b} (%) 1b[2b]		ε_{R_c} (%) 1c[2c]	
	$D = 1\ m$	$D = 2\ m$	$D = 1\ m$	$D = 2\ m$	$D = 1\ m$	$D = 2\ m$
0	12.7 [25.5]	1.3 [4.3]	33.1 [43.6]	17.6 [15.0]	5.5 [1.4]	26.9 [30.4]
1	26.3 [15.1]	10.7 [24.3]	23.4 [3.7]	33.4 [23.2]	11.3 [13.3]	22.5 [26.6]
2	21.1 [0.3]	23.5 [45.6]	45.0 [38.9]	57.9 [75.0]	30.3 [38.8]	11.2 [14.5]
3	25.4 [26.2]	0.1 [14.3]	28.4 [28.2]	11.4 [8.5]	28.7 [31.0]	29.9 [10.8]
4	30.9 [6.9]	23.0 [4.2]	18.5 [21.5]	17.9 [5.7]	9.6 [16.1]	28.0 [10.9]
5	22.2 [31.8]	1.8 [1.2]	25.4 [20.3]	11.0 [19.3]	16.0 [3.6]	21.0 [30.0]

For wind speed $U_0 = 1$ & 2 m/s cases, the fire decelerates as it approaches each other due to wind inhibiting its approach towards each other driving it in the X-direction keeping an equilibrium between wind and buoyancy force. When a fireline burns, the flame was almost vertical and mainly directed along the wind due to the equilibrium between two forces. Later, the fire slowly creeps towards the other fireline. It can be seen from supplementary videos (SV1 and SV2) that these two cases required more time as compared to other cases to merge.

At high wind speed cases, the ROS accelerates even when higher wind speed due to increased combustion process as preheating of fuel bed by the convective and radiative heat load and increased turbulence. This phenomenon is visible in the growth of fire observed for $U_0 = 5$ m/s at 2 m spacing in Fig. 4(e)-(h) and was discussed earlier. When both firelines burnt, the flames of each fireline lean towards each other, the flame angle decreased, and the ROS increased as they approach each other. The effect of the stronger wind intensified the overall fire behaviour so the heat from the two approaching flame fronts can predominate over the residual heat in-draft from the burnt area, leading to stronger flow convergence between the two approaching fire lines. This phenomenon was also observed by Viegas *et al.* (2021) in oblique-shaped fires.

It was also observed in Fig. 8 and 9 that the maximum and minimum fire spread rates were higher and lower than most of the experimentally reported values for the same. The most likely reason for this issue was the temporal scale of simulation measurement which was significantly smaller than the experiment. The smaller resolution was selected to provide better information which was one of the challenges in the experimental study. The simulated fireline can move instantaneously in the opposite direction (to the mean spread) or can stay approximately at the same grid cell. This yields a negative ROS value or a ROS value close to zero. The fire accelerated significantly faster in the short period to yield a very high value for the ROS (Supplementary videos SV1 and SV2 provide greater insight into this behaviour). Usually, a higher variation between the maximum and minimum ROS was observed on the measuring line ‘b’ and ‘c’ than ‘a’ due to preheating of vegetative fuel by part of the flame near measuring lines ‘a’ and ‘b’ respectively.

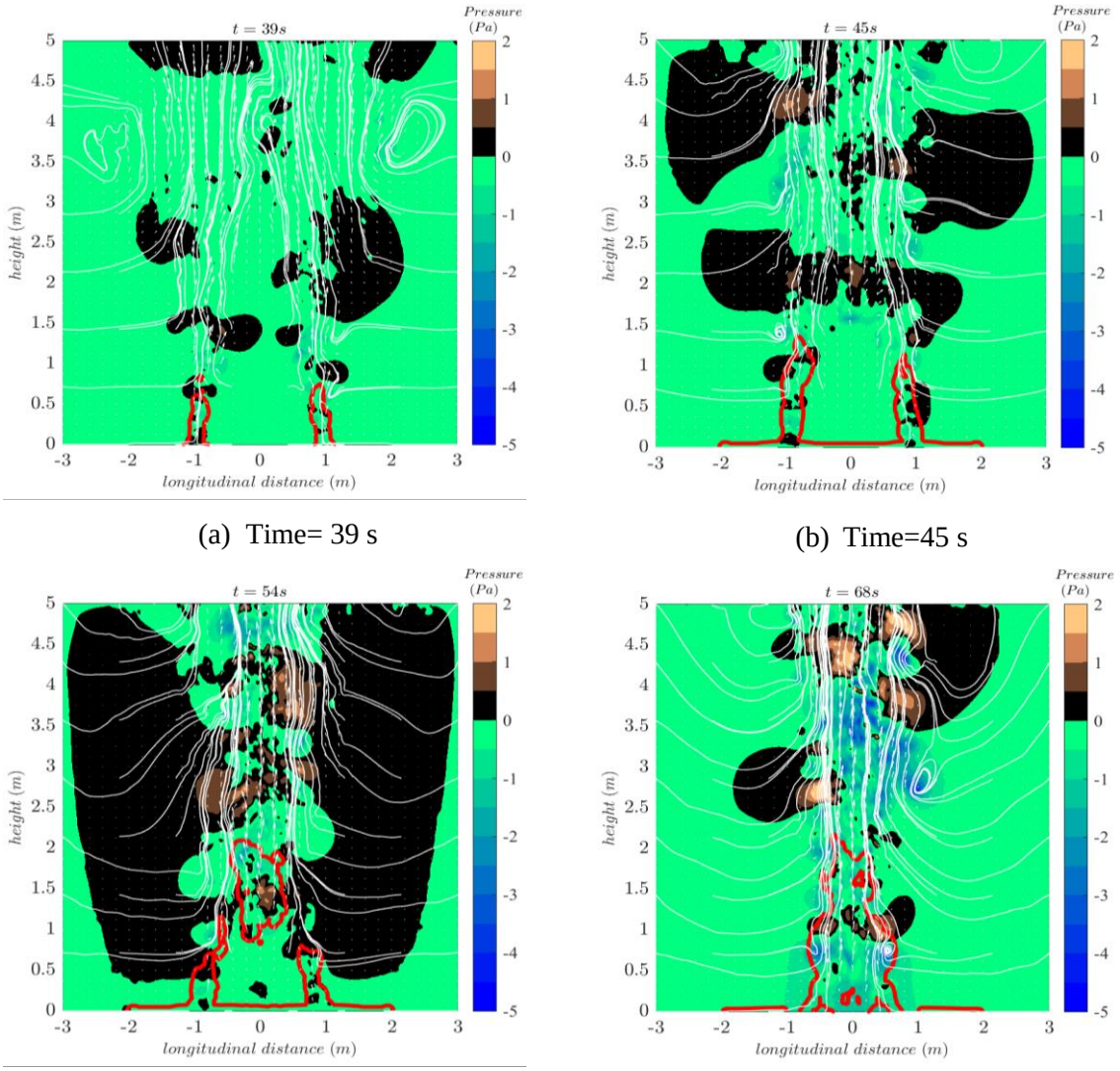

(a) Time= 39 s

(b) Time=45 s

(c) Time =54 s

(d) Time = 68s

Fig. 10: Variation of pressure with time along the measuring line 'b' ($X = 3m$) for $U_0 = 0m/s$ at spacing of 2 m. Streamlines and quivers represent the direction of velocity in YZ plane and solid red line represents the flame location is based on 90% of heat release rate per unit volume.

Furthermore, it can be observed from the supplementary videos that the flame geometry and size changes as the two fire fronts advance and are significantly dependent on the role of horizontal and vertical forces acting on the fire front (Morvan 2007; Balbi *et al.* 2020; Viegas *et al.* 2021). Consequently, the rate of fire spread changes significantly dependent on two forces. Moreover, the average rate of fire spread (R_{avg}) which is based on the average ROS measured along the three measuring lines at both spacings (1 and 2 m) with the wind speed shown in Fig. 11. It shows a non-monotonic behaviour with minima observed for R_{avg} with wind velocity between U_0= 1 and 3 m/s.

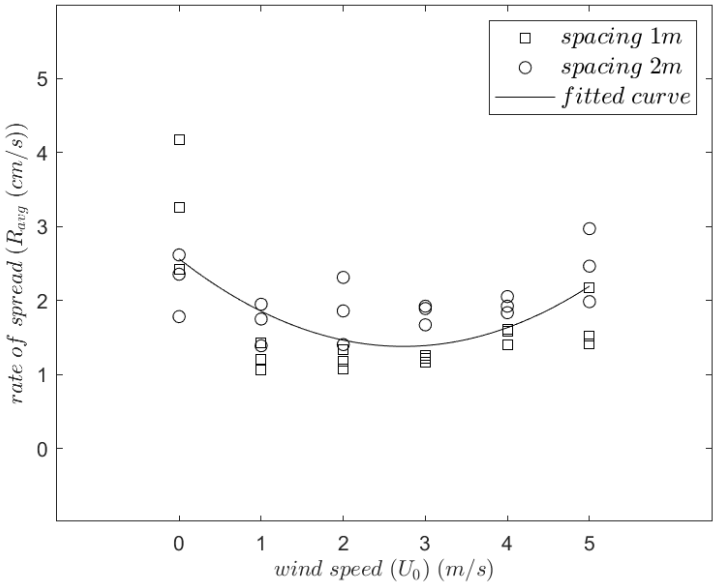

Fig. 11: The average ROS (R_{avg}) as a function of the wind flow velocity U_0 (0–5 m/s) for both spacing between the firelines.

The data set was found to fit a quadratic equation given by,

$$R_{avg} = 0.158U_0^2 - 0.866U_0 + 2.563, \quad \text{Eq. 9}$$

with the goodness of fit, $r^2 = 0.81$. It is important to be aware that this equation is a specific fit to this idealised simulation data set and may not immediately generalise to other scenarios. Note that factors such as scale, topography, fuel heterogeneity, driving wind and wind changes will significantly affect the R_{avg} of a real parallel merging fire.

The information from these and future studies will be helpful in assisting the operational fire community developing a better understanding of physics-behind and factors controlling the parallel strip prescribed burning practices adopted mainly in grassland management (McRae 1996). McRae (1996) observed that during the strip burning practices in information of local wind speed is difficult to quantify and reliance of ambient wind is limited once the convective column develop. The eddies form between the two firelines under certain condition could give rise to extreme behaviour such as fire whirl. The knowledge from a detailed physics-based model could help understand such behaviour and provide a better understanding of strip burning practices. Scale-up of the present work would provide an accomplishable approach to these complex fire behaviours which are arduous for fire fighters to obtain useful insight and data collection during the burning practices.

A few experimental studies have tried to develop some correlation but only at lab-scale for merging fires under a limited set of ambient conditions (Viegas *et al.* 2012; Viegas *et al.* 2013; Raposo *et al.* 2018; Viegas *et al.* 2021; Li *et al.* 2022; Ribeiro *et al.* 2022; Ribeiro *et al.* 2023). However, their application at a field scale is still under scrutiny. For example, Sullivan *et al.* (2019) observed a significantly different behaviour of oblique-shaped merging fire when they considered eucalyptus

leaves with bark and twigs over traditional straw or pine needles based oblique shaped merging fire. Physics-based fire model can fill this gap and test the efficacy of those correlation especially at a plot scale typically of the order of a few hundred meters. Nevertheless, a robust numerical simulation and its validation exercise is further required with the experimental measurement when scaling up to arrive at a meaningful practical reduced order correlation that can be used in operational fire models which assumes quasi-steady approach on fire behaviour. Merging fires are a dangerous dynamic fire phenomenon that can sharply increase fire spread rate, and it is imperative that it is accounted appropriately in the operational fire models.

Conclusions

The interaction of two parallel fire fronts initially separated by a distance spreading laterally in a parallel flow under different wind velocities is studied using a physics-based fire model. We observed that the rate of fire spread of approaching parallel fire shows a non-monotonic relationship with the wind speed. In the absence of wind, the rate of fire spread of the two approaching fires has a relatively high value that decreases with increasing wind velocity, reaching a minimum value for a range of relatively low values of wind velocity, and then increasing with wind velocity. Most of the numerically estimated rates of fire spread in our study are found to have a relative error of 5-35% with the experimentally observed rate of fire spread. A higher relative error is observed when the experimental rate of spread is low.

The present study serves as a key benchmark case study for a physics-based fire model that will help expand the understanding of the behaviour of parallel fire interaction with ambient conditions. The derived benefit of validated physics-based fire model to investigate various factors controlling the merging fire behaviour which are difficult to control even in controlled experiment and providing a cost-effective alternative to experimental studies.

The impetus of the present study can expand the validated physics-based fire model on homogeneous vegetation bed to investigate non-homogeneous vegetation especially the irregular shaped leaves (e.g., eucalyptus) or mixed fuel type (that includes barks and twigs). Future work focusing on the development of reduced order correlations between the merging of two or more fires can amplify the practical application of knowledge learnt utilising a physics-based fire model. These correlations could be incorporated into operational fire models that assumes that the rate of fire spread is not affected by the merging fire behaviour.

Acknowledgement

The authors also wish to acknowledge the computational resource utilised at the University Research Facility in Big Data Analytics (UBDA) platform, The Hong Kong Polytechnic University, Hong Kong, and National Computational Infrastructure (NCI), University of New South Wales, Australia.

Declaration of Funding

This work is funded by the Hong Kong Research Grants Council Theme-based Research Scheme (T22-505/19-N) and National Natural Science Foundation of China (No. 52322610).

Declaration of Competing Interest

The authors declare that there is no conflict of interest between each other. Dr Xinyan Huang is an Associate Editor of the International Journal of Wildland Fire. To mitigate this potential conflict of interest he was blinded from the review process and was not involved at any stage in the editing of this manuscript.

Data Availability Statement

The data that support this study will be shared upon reasonable request to the corresponding author.

References:

Balbi, JH, Chatelon, FJ, Morvan, D, Rossi, JL, Marcelli, T, Morandini, F (2020) A convective–radiative propagation model for wildland fires. *International Journal of Wildland Fire* **29**, 723-738.

Billing, P (1987) Heathcote Fire Bendigo Fire No. 38-1986-87. Fire Management Branch, Department of Conservation, Forests and Lands, Report No. 27, Victoria, Australia.

Blanchi, R, Leonard, J (2005) Investigation of Bushfire Attack Mechanisms Resulting in House Loss in the ACT Bushfire 2003, A Bushfire Cooperative Research Centre (CRC) Report. CMIT Technical Report-2005.

Cheney, N, Gould, J, Catchpole, W (1993) The influence of fuel, weather and fire shape variables on fire-spread in grasslands. *International Journal of Wildland Fire* **3**, 31-44.

Cruz, MG, Gould, JS, Alexander, ME, Sullivan, AL, McCaw, WL, Mathews, S (2015) 'Guide to Rate of Fire Spread Models for Australian Vegetation.' (CSIRO Land and Water Flagship, Canberra, ACT and AFAC, Melbourne, VIC:

De Groot, WJ, Alexander, ME (1986) 'Wildfire behavior on the Canadian Shield: a case study of the 1980 Chachukew fire, east-central Saskatchewan. , Third Central Region Fire Weather Committee Scientific and Technical Seminar.' Winnipeg, Manitoba, 3rd April 1986. (Northern Forestry Centre, Canadian Forest Service, Natural Resources Canada, Edmonton, Alberta:

Filkov, A, Cirulis, B, Penman, T (2020) Quantifying merging fire behaviour phenomena using unmanned aerial vehicle technology. *International Journal of Wildland Fire* **30**, 197-214.

Finney, MA, McAllister, SS (2011) A Review of Fire Interactions and Mass Fires. *Journal of Combustion* **2011**, 548328.

Graham, RT (2003) 'Hayman fire case study.' (US Department of Agriculture, Forest Service, Rocky Mountain Research Station:

Halofsky, JE, Peterson, DL, Harvey, BJ (2020) Changing wildfire, changing forests: the effects of climate change on fire regimes and vegetation in the Pacific Northwest, USA. *Fire Ecology* **16**, 1-26.

Hassan, A, Accary, G, Sutherland, D, Moinuddin, K (2023) Physics-based modelling of junction fires: parametric study. *International Journal of Wildland Fire* **32**, 336-350.

Hurley, MJ, Gottuk, DT, Hall Jr, JR, Harada, K, Kuligowski, ED, Puchovsky, M, Watts Jr, JM, Wieczorek, CJ (2015) 'SFPE handbook of fire protection engineering.' (Springer: New York)

Jarrin, N (2008) Synthetic inflow boundary conditions for the numerical simulation of turbulence. PhD thesis, The University of Manchaster, United Kingdom.

Khan, N, Sutherland, D, Wadhwani, R, Moinuddin, K (2019) Physics-based simulation of heat load on structures for improving construction standards for bushfire prone areas. *Frontiers in Mechanical Engineering* **5**, 35.

Li, K, Ma, Z, Huang, X, Zou, Y (2022) Merging dynamics of dual parallel linear diffusion flames. *Fire safety journal* **127**, 103490.

Li, M, Shen, F, Sun, X (2021) 2019–2020 Australian bushfire air particulate pollution and impact on the South Pacific Ocean. *Scientific Reports* **11**, 1-13.

Linn, R, Reisner, J, Colman, JJ, Winterkamp, J (2002) Studying wildfire behavior using FIRETEC. *International Journal of Wildland Fire* **11**, 233-246.

Liu, N, Lei, J, Gao, W, Chen, H, Xie, X (2021) Combustion dynamics of large-scale wildfires. *Proceedings of the Combustion Institute* **38**, 157-198.

Manzello, SL, Suzuki, S, Gollner, MJ, Fernandez-Pello, AC (2020) Role of firebrand combustion in large outdoor fire spread. *Progress in Energy and Combustion Science* **76**, 100801.

McGrattan, K, Hostikka, S, Floyd, J, McDermott, R, Vanella, M (2022a) Fire dynamics simulator (Sixth Edition) user's guide. National Institute of Standards and Technology, Gaithersburg, Maryland, USA.

McGrattan, K, Hostikka, S, Floyd, J, McDermott, R, Vanella, M (2022b) Fire Dynamics Simulator Technical Reference Guide Volume 1: Mathematical Model. National Institute of Standards and Technology, Gaithersburg, Maryland, USA.

McRae, DJ (1996) Prescribed fire aerial ignition strategies. Natural Resources Canada, Canadian Forest Service, Great Lakes Forestry Centre No. NODA/NFP Technical Report TR-33, Ontario, Canada.

Mell, W, Charney, J, Jenkins, MA, Cheney, P, Gould, J (2013) Numerical simulations of grassland fire behavior from the LANL-FIRETEC and NIST-WFDS models. In 'Remote Sensing and Modeling Applications to Wildland Fires.' pp. 209-225. (Springer: Beijing)

Mell, W, Jenkins, MA, Gould, J, Cheney, P (2007) A physics-based approach to modelling grassland fires. *International Journal of Wildland Fire* **16**, 1-22.

Moinuddin, K, Sutherland, D (2019) Modelling of tree fires and fires transitioning from the forest floor to the canopy with a physics-based model. *Mathematics and Computers in Simulation* **175**, 81-95.

Moinuddin, K, Sutherland, D, Mell, W (2018) Simulation study of grass fire using a physics-based model: striving towards numerical rigour and the effect of grass height on the rate of spread. *International Journal of Wildland Fire* **27**, 800-814.

Morvan, D (2007) A numerical study of flame geometry and potential for crown fire initiation for a wildfire propagating through shrub fuel. *International Journal of Wildland Fire* **16**, 511-518.

Morvan, D, Hoffman, C, Rego, F, Mell, W (2011) Numerical simulation of the interaction between two fire fronts in grassland and shrubland. *Fire safety journal* **46**, 469-479.

Parente, J, Pereira, M, Amraoui, M, Fischer, EM (2018) Heat waves in Portugal: Current regime, changes in future climate and impacts on extreme wildfires. *Science of the total environment* **631**, 534-549.

Perez-Ramirez, Y, Mell, WE, Santoni, P-A, Tramoni, J-B, Bosseur, F (2017) Examination of WFDS in Modeling Spreading Fires in a Furniture Calorimeter. *Fire Technology* **53**, 1795-1832.

Raposo, J, Viegas, D, Xie, X, Almeida, M, Figueiredo, A, Porto, L, Sharples, J (2018) Analysis of the physical processes associated with junction fires at laboratory and field scales. *International Journal of Wildland Fire* **27**, 52-68.

Ribeiro, C, Reis, L, Raposo, J, Rodrigues, A, Viegas, DX, Sharples, J (2022) Interaction between two parallel fire fronts under different wind conditions. *International Journal of Wildland Fire* **31**, 492-506.

Ribeiro, C, Viegas, DX, Raposo, J, Reis, L, Sharples, J (2023) Slope effect on junction fire with two non-symmetric fire fronts. *International Journal of Wildland Fire*

Ronchi, E, Gwynne, S, Rein, G, Wadhwani, R, Intini, P, Bergstedt, A (2017) e-Sanctuary: Open Multi-Physics Framework for Modelling Wildfire Urban Evacuation. Fire Protection Research Foundation No. FPRF-2017-22, Quincy, MA, USA.

San-Miguel-Ayanz, J, Oom, D, Artes, T, Viegas, D, Fernandes, P, Faivre, N, Freire, S, Moore, P, Rego, F, Castellnou, M (2020) Forest fires in Portugal in 2017. *Science for Disaster Risk Management*

Sharples, J, Viegas, D, McRae, R, Raposo, J, Farinha, H (2011) 'Lateral bushfire propagation driven by the interaction of wind, terrain and fire., 19th International Congress on Modelling and Simulation.' Perth, Australia.

Sharples, JJ, Cary, GJ, Fox-Hughes, P, Mooney, S, Evans, JP, Fletcher, M-S, Fromm, M, Grierson, PF, McRae, R, Baker, P (2016) Natural hazards in Australia: extreme bushfire. *Climatic change* **139**, 85-99.

Sullivan, AL (2009) Wildland surface fire spread modelling, 1990–2007. 1: Physical and quasi-physical models. *International Journal of Wildland Fire* **18**, 349-368.

Sullivan, AL, Swedosh, W, Hurley, RJ, Sharples, JJ, Hilton, JE (2019) Investigation of the effects of interactions of intersecting oblique fire lines with and without wind in a combustion wind tunnel. *International Journal of Wildland Fire* **28**, 704-719.

Tedim, F, Leone, V, Amraoui, M, Bouillon, C, Coughlan, MR, Delogu, GM, Fernandes, PM, Ferreira, C, McCaffrey, S, McGee, TK (2018) Defining extreme wildfire events: difficulties, challenges, and impacts. *Fire* **1**, 9.

Thomas, C, Sharples, J, Evans, J (2017) Modelling the dynamic behaviour of junction fires with a coupled atmosphere–fire model. *International Journal of Wildland Fire* **26**, 331-344.

Tomshin, O, Solovyev, V (2022) Features of the Extreme Fire Season of 2021 in Yakutia (Eastern Siberia) and Heavy Air Pollution Caused by Biomass Burning. *Remote Sensing* **14**, 4980.

Vanella, M, McGrattan, K, McDermott, R, Forney, G, Mell, W, Gissi, E, Fiorucci, P (2021) A Multi-Fidelity Framework for Wildland Fire Behavior Simulations over Complex Terrain. *Atmosphere* **12**, 273.

Viegas, D, Raposo, J, Figueiredo, A (2013) Preliminary analysis of slope and fuel bed effect on jump behavior in forest fires. *Procedia Engineering* **62**, 1032-1039.

Viegas, DX, Raposo, JR, Davim, DA, Rossa, CG (2012) Study of the jump fire produced by the interaction of two oblique fire fronts. Part 1. Analytical model and validation with no-slope laboratory experiments. *International Journal of Wildland Fire* **21**, 843-856.

Viegas, DXFC, Raposo, JRN, Ribeiro, CFM, Reis, LCD, Abouali, A, Viegas, CXP (2021) On the non-monotonic behaviour of fire spread. *International Journal of Wildland Fire* **30**, 702-719.

Wadhwani, R (2019) Physics-based simulation of short-range spotting in wildfires. PhD thesis, Victoria University.

Wadhwani, R, Sullivan, C, Wickramasinghe, A, Kyng, M, Khan, N, Moinuddin, K (2022) A review of firebrand studies on generation and transport. *Fire safety journal* 103674.

Werth, PA, Potter, BE, Clements, CB, Finney, MA, Forthofer, JA, McAllister, SS, Goodrick, SL, Alexander, ME, Cruz, MG (2011) Synthesis of knowledge of extreme fire behavior: volume I for fire managers.